SCIENCE CHINA
Technological Sciences

• Article •

November 2016 Vol.59 No.11: 1777–1784
doi: 10.1007/s11431-015-0778-0

Behaviors of field emitters under pulsed voltages

YANG Jin[1,2] & ZHANG GengMin[1,3*]

[1]*Key Laboratory for the Physics and Chemistry of Nanodevices and Department of Electronics, Peking University, Beijing 100871, China;*
[2]*Academy for Advanced Interdisciplinary Studies, Peking University, Beijing 100871, China;*
[3]*SIP-UCLA Institute for Technology Advancement, Suzhou 215123, China*

Received March 30, 2016; accepted June 16, 2016; published online September 13, 2016

In this paper we described our study of the behaviors of field emitters driven by square-wave voltages. We observed phenomena under pulsed voltages that generally do not manifest themselves under direct-current voltages. We interpreted these phenomena with the cathode and anode combined treated as equivalent to a resistor and a condenser in series connection. First, because of the delay caused by the charging process of the condenser, the waveform of the voltage across the cathode-anode gap was remarkably distorted. Second, the resistor led to considerable attenuation in field emission, which was clearly observable within each pulse and became more dramatic with increasing repetition frequency of the pulses. Furthermore, the field emission currents under direct-current voltages were lower than those under pulsed voltages. This disparity is attributed to rising resistance in the circuit with rising temperature. We also discussed the restrictions that the waveform distortion and current attenuation could impose on potential field emitter applications.

field emission, pulsed voltage, charging current, attenuation, waveform distortion

Citation: Yang J, Zhang G M. Behaviors of field emitters under pulsed voltages. Sci China Tech Sci, 2016, 59: 1777–1784, doi: 10.1007/s11431-015-0778-0

1 Introduction

Great efforts have been devoted to studying field emission in the search for ideal cold electron sources. Except for traditional Spindt-type field emitter arrays, many nanomaterials, e.g., carbon nanotubes and semiconductor nanomaterials, can also deliver electron beams under strong electric fields [1–10]. Within our knowledge, most field emission research is currently performed under direct-current (DC) voltages. However, in many applications, field emitters work under pulsed voltages. In some cases, DC field emission cannot meet requirements, and pulsed field emission is therefore necessary. In other cases, pulsed field emission is preferable to DC field emission. In the past, researchers have attempted to develop field emission displays, and some of them are continuing these attempts [11]. Because of the persistence of vision, field emitters do not need to remain on throughout the operation of a field emission display. Today, the application of field emitters in X-ray tubes is promising [12]. As long as the intensity of the X-ray radiation is not required to be high, it is recommended that the tube is operated under a pulsed voltage, so that the patient and/or the operator will be exposed to less X-ray irradiation. It is also hoped that traditional thermionic cathodes can be replaced by cold electron sources in microwave tubes, and some progress has already been made by directly driving a cold emitter using an electromagnetic field [13]. Moreover, in all potential applications, if a field emitter can be operated under a pulsed voltage, its actual working time can be reduced in comparison with operating it under a DC voltage, so that its nominal lifetime can be prolonged.

For these reasons, the behaviors of field emitters under pulsed voltages are worth studying. A field emitter can behave differently under pulsed voltages than under DC volt-

*Corresponding author (email: zgmin@pku.edu.cn)

ages. As a reference, it might be interesting to refer to the oxide cathode, which is one of the most important thermionic cathodes. Matheson and Nergaard [14] argued: "It is a common observation that the pulsed and DC emissions from an oxide cathode in an ordinary vacuum tube differ by about an order of magnitude". Pulsed field emission also has some peculiarities. The present paper focuses on two of these: the role of the charging current and the dramatic decay of the emissive current inside a pulse.

2 Experimental methods

2.1 Sample preparation

We used two types of samples as the field emitters: multi-walled carbon nanotubes (MWCNTs) and titanium dioxide (TiO_2) nanotubes. Both the substrates of the two emitters in the field emission measurement were n-type Si wafers.

Commercial MWCNTs (XFNANO) were dispersed in deionized water with a 0.2 mg/mL concentration and subjected to ultrasonic treatment for 12 h. After standing for another 12 h, the supernatant fluid from the suspension was applied to a cleaned Si wafer substrate (2.3 mm × 3.0 mm and thickness 0.5 mm). Then the MWCNTs were attached to the Si substrate after evaporation of the water.

TiO_2 nanotube arrays were fabricated with a two-step anodization method, details of which can be found in ref. [15]. Ethylene glycol ($C_2H_6O_2$) containing 75 mmol/L ammonium fluoride (NH_4F) and 0.2 mol/L water was used as the electrolyte in the anodization after 2 h of stirring. Ti foil of thickness 0.25 mm and 99.7% purity was ultrasonically cleaned in, in turn, deionized water, acetone, and isopropanol and then attached to a Cu plate connected to the positive electrode of a DC power source. A graphite sheet was connected to the negative electrode of the power source. The Ti foil and the graphite sheet were inserted into the electrolyte, and a 60 V DC voltage was applied between them. This anodization was performed twice. After 24 h of anodization, the Ti foil was fetched out from the electrolyte, and the nanotube array on its surface was removed ultrasonically. After this removal, well-ordered imprints were left on the foil surface. Then the Ti foil was reinserted into the electrolyte for another 12 h anodization. In the second-step anodization, the imprints served as the template for further growth of the TiO_2 nanotubes, so that the orderliness of the nanotubes was guaranteed.

Because the Ti foil surface was not sufficiently flat for field emission measurement, the TiO_2 nanotube array of thickness 21 μm was detached from the Ti foil and pasted onto a Si substrate (1.8 mm × 1.8 mm and thickness 0.5 mm) with colloidal graphite.

2.2 Field emission measurement

We measured the field emission behaviors of the samples in a laboratory-built ultrahigh vacuum system under a base pressure of 10^{-7}–10^{-8} Pa. In each measurement, the sample was fixed on a Mo holder and used as the cathode. The cathode surface was separated from the stainless-steel anode by 0.20–0.25 mm. We applied either a DC high voltage (H.V.) or a pulsed H.V. with a square-shaped waveform to the cathode-anode gap. The duration of a pulse and the repetition rates of the pulses ranged from 5 to 50 μs and 0.2 to 1.0 kHz, respectively.

When a DC H.V. was applied, we used an ammeter to record the current in the circuit. When a pulsed H.V. was applied, we used an oscilloscope to record the voltage across a non-inductive sampling resistor (2 or 10 kΩ) in the circuit every 10 ns, and we calculated the current flowing through the sampling resistor accordingly. We used the "Average Mode" of the oscilloscope to improve the signal-to-noise ratio and voltage resolution.

3 Results and discussion

3.1 MWCNT and TiO_2 field emitters

Figure 1(a) and (b) shows the MWCNTs on the Si substrate. Their average diameter was 5×10^1 nm. Although they were not well aligned, some parts (indicated by the circles in Figure 1(a)) displayed an upward orientation. These upward MWCNT parts may have acted as field emitters when strong fields were applied. Figure 1(c) and (d) shows that the TiO_2 nanotubes had a pore diameter of approximately 0.2 μm and were well ordered. As shown in the inset of Figure 1(c), electron emission would be available from the sharp edges and the sharp tips at the boundaries shared by the contiguous nanotubes under strong electric fields [16]. Because the pulsed and DC voltages applied in this work were only moderately high and the extracted field emission currents were not particularly large, the field emission tests did not lead to obvious damage to the samples (Figure 1(b) and (d)).

3.2 Role of the displacement current

Figure 2 shows the measurement circuit and its equivalent circuits.

When the system was in a steady state, the current was spatially continuous throughout the system (here the word "current" is used to denote the current caused by the movement of charges. In some literatures, it is more specifically called the "charge current" so that it can be unambiguously distinguished from the displacement current). That is, the current measured in the circuit was equal to the emissive current between the cathode and the anode, which arose from the electron emission from the cathode. In contrast, at the beginning and end of a pulse, when the voltage changed with time dramatically, the whole system was in a transient

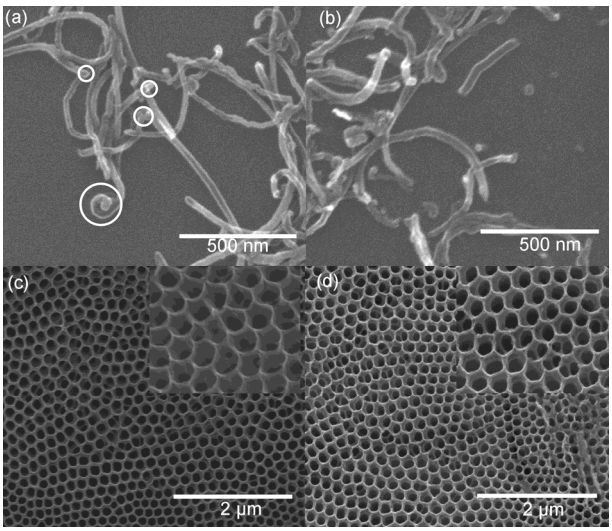

Figure 1 MWCNTs and TiO_2 nanotubes on Si wafer substrates. (a), (b) MWCNTs; (c), (d) TiO_2 nanotubes. (a), (c) Before the field emission measurements; (b), (d) after the measurements.

state, and hence displacement current came into play and a generalized continuity relationship replaced the continuity of the charge current. In this case, the current measured in the circuit was actually equal to the sum of the emissive current and the displacement current between the cathode and the anode. In other words, part of the current in the circuit was devoted to replenishing the emitted electrons from the cathode and the other part was devoted to charging the cathode–anode condenser. This relationship is expressed as

$$I_s = I_e + I_c, \tag{1}$$

where I_s is the current measured in the circuit ("s" for "sum"), I_e is the emissive current ("e" for "emissive"), and I_c is the displacement current, namely the charging current ("c" for "charging"). At the beginning of a pulse, the condenser underwent a charging process and I_c was positive. At the end of a pulse, the condenser underwent a discharging process and I_c was negative.

The power source output a chain of square-wave pulses, whose rise time and fall time were both less than 1 μs. Thus the square pulses can be treated as step functions of time. Because the fall time was greater than the rise time, we paid more attention to the rising edges of the pulses.

The waveform of the voltage across the cathode-anode gap was inevitably distorted from the square shape because of the charging process. The voltage across the cathode-anode gap, denoted by V_C, rose to V_0 in a process whose duration is characterized by the time constant $\tau = RC$:

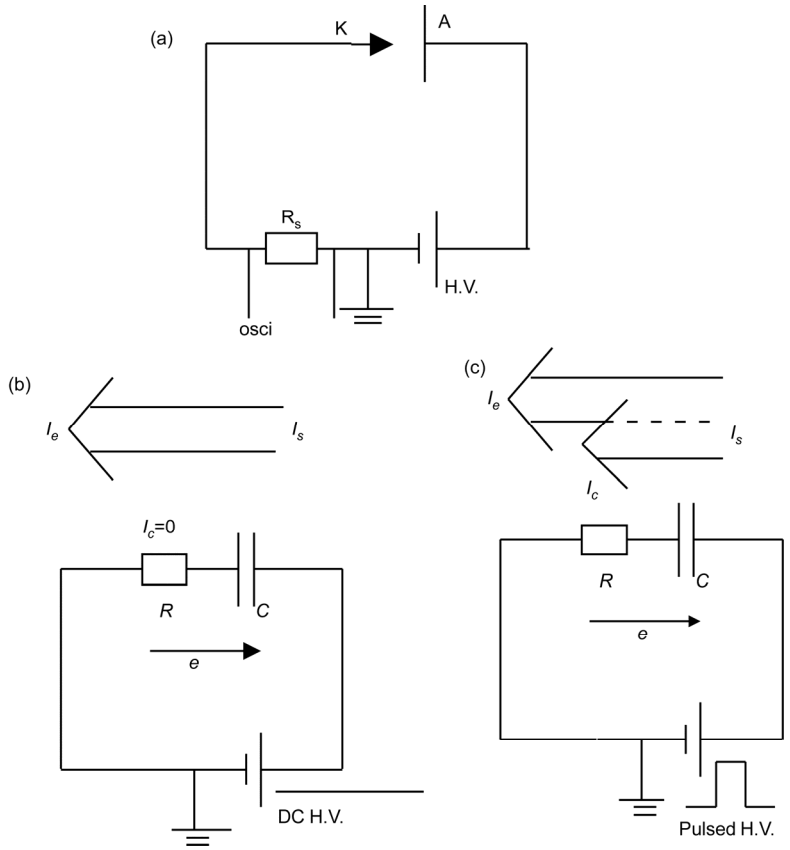

Figure 2 The measurement circuit and its equivalent circuits (K, cathode; A, anode; R_s, sampling resistor; e, direction of the electron flow; osci, oscilloscope). (a) The measurement circuit; (b) the equivalent circuit under the DC voltages; and (c) the equivalent circuit under the pulsed voltages.

$$V_{\mathrm{C}} = V_0\left(1-\mathrm{e}^{-\frac{t}{RC}}\right) = V_0\left(1-\mathrm{e}^{-\frac{t}{\tau}}\right), \tag{2}$$

where V_0 is the magnitude of the pulsed voltage; R is the sum of all the resistances in the circuit, including mainly those of the emitter, the emitter-substrate interface, and the sampling resistor; C is the capacitance between the cathode and the anode; and t is the time counted from the starting instant of the pulse.

Because it was difficult to measure directly the voltage across the cathode-anode gap, the charging current at the beginning of a pulse was studied instead:

$$I_{\mathrm{c}} = C\frac{\mathrm{d}V_{\mathrm{C}}}{\mathrm{d}t} = \frac{V_0}{R}\mathrm{e}^{-\frac{t}{\tau}}. \tag{3}$$

When a stable high voltage was established across the gap, i.e., the voltage became constant, the charging current should vanish. When the voltage was still too low to extract significant field emission from the cathode, the current measured in the circuit was equal to the charging current:

$$I_{\mathrm{s}} = I_{\mathrm{c}}. \tag{4}$$

Figure 3 shows two waveforms of I_{s} measured in the circuit under low-voltage pulses when field emission was yet to occur.

Using the value of the charging current at the starting instant $I_{\mathrm{c}}(0) = \frac{V_0}{R}$, which can be readily estimated from the measurement results (Figure 3), the R values of the two samples are respectively calculated.

Then, by measuring the time for the currents to drop from $I_{\mathrm{c}}(0)$ to $\frac{I_{\mathrm{c}}(0)}{e}$, the values of the time constant τ are obtained, and subsequently the values of τ and R are used to calculate the C values.

Alternatively, the capacitance of a parallel-plate capacitor can be approximately calculated using the formula:

$$C = \varepsilon_0\frac{S_{\mathrm{C}}}{d}, \tag{5}$$

where ε_0 is the vacuum permittivity, S_{C} is the area of the two plates, and d is the separation between the two plates. Because the area of the cathode was obviously smaller than the area of the anode, here the area of the cathode is used as the S_{C} value. Table 1 shows the results of all these calculations.

The disparity between the R values listed in Table 1 is not particularly dramatic despite the fact that the resistance of the MWCNTs and TiO_2 nanotubes should clearly differ. This similarity in the R values indicates that the resistances at the emitter-substrate interfaces played a more important role than the resistances of the emitters themselves in determining the R values. The high resistance of the emitter-substrate interface is attributable to the partial oxidation of the Si wafer surfaces. The C values calculated by using the $I_{\mathrm{s}} = I_{\mathrm{c}}$ waveforms are larger than those calculated using eq. (5) of the parallel-plate capacitor model. This disparity is mainly attributable to the fact that the parasitic capacitance in the equivalent circuit also arose from other components of the circuit except for the cathode and anode plates.

3.3 Temporal characteristics of the emission

We studied the temporal characteristics of the emissive currents in three aspects: (1) the waveforms in individual pulses; (2) the dependence of the average emissive currents on the repetition rates; and (3) a comparison of the current-voltage relationships under pulsed and under DC H.V.

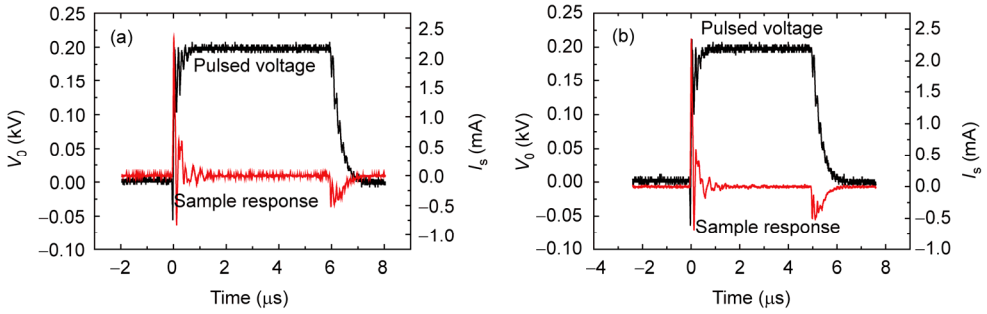

Figure 3 (Color online) Current waveforms acquired in the circuit in the absence of field emission. V_0 = 200 V. (a) MWCNT/Si, T_0 = 6 μs; (b) TiO_2 nanotubes, T_0 = 5 μs. T_0 is the pulse duration.

Table 1 The R and C values of the cathode-anode system[a)]

Emitter	d (mm)	S_{C} (mm^2)	$R(k\Omega) = \frac{V_0}{I(0)}$	τ (μs) ($I(\tau) = \frac{I(0)}{e}$)	$C(\mathrm{pF}) = \frac{\tau}{R}$	$C(\mathrm{pF}) = \varepsilon_0\frac{S_C}{d}$
MWCNT/Si	0.20	2.3 × 3.0	70	0.056	0.80	0.31
TiO_2/Si	0.16	1.8 × 1.8	75	0.11	1.4	0.18

a) The C values are respectively calculated by using the I_{c} waveform shown in Figure 3 and the parameters of the equivalent parallel-plate capacitor.

Figure 4 shows the waveforms of the measured current densities (J_s-t curves) under high voltages, where J_s is attained simply by dividing I_s by the cathode area. When the voltage was sufficiently high in a test, I_e began to occur and I_c rose accordingly. As a result, I_s (and J_s) became so large at the beginning and end of a pulse that it went beyond the range of the oscilloscope. It was measurable only after at least 2 μs from the beginning of the pulse. From the calculation results shown in Table 1 it is known that the time constants of both the MWCNT and the TiO_2 emission systems were much smaller than 2 μs. That is, 2 μs after the beginning of a pulse, the contribution by the charging current to the total current measured in the circuit was actually negligible. Therefore, in a waveform, except for the invisible parts that go beyond the range of the oscilloscope at the beginning and end of the pulse, the part that is well displayed on the oscilloscope all originates from the emissive current. In particular, the dramatic attenuation in the first half of the pulse, as indicated by the arrows in Figure 4, did not arise from the attenuation of the charging current. Instead, it reflects the considerable drop of the emissive current in the first half of a pulse. The current almost stabilizes in the second half of the pulse. However, even in the second half, the J_s-t curves are still not strictly horizontal. Instead, both curves have negative slopes, which are more visible in the insets to Figure 4. The results shown in Figure 4 indicate that the attenuation of the emissive currents could be a serious concern in practical applications.

The fact that the emissive current decayed considerably in a pulse (Figure 4) indicates the necessity of finding an appropriate quantity for characterizing the field emission capability of a sample under H.V. pulses. In this work, the "average emissive current" of a sample under pulsed voltages is defined as the average value of the emissive currents in the second half of a pulse before discharging at the end of the pulse. Such a quantity is introduced for the following two reasons. First, the first half contained both the charging current and the emissive current, and they both decayed dramatically. Second, the relatively stable emission in the second half of the pulse still decayed slowly, and thus the average must be used.

Accordingly, in the calculation of the "turn-on field" (E_{on}) and the "threshold field" (E_{th}) of a sample, the values of the "average emissive currents" are used for the results obtained under pulsed voltages. Following common practice, the "turn-on field" is defined as the average field between the cathode and the anode for extracting a 10 μA/cm^2 current density. The "threshold field" is defined as the average field for extracting a 1 mA/cm^2 current density [4,17]. In the present work, following common practice, both E_{on} and E_{th} were obtained simply by dividing the output voltages of the voltage source at the current densities 10 μA/cm^2 and 1 mA/cm^2, respectively, by the cathode-anode separation. Thus, strictly speaking, they were not genuine "average fields" between the cathode and the anode, because the voltage drop caused by R in the circuit led the actual voltages across the cathode-anode gap to be lower than the output voltages from the voltage source.

The average emissive currents of the two samples also decreased with an increasing repetition frequency of the pulses (Figure 5).

Also noteworthy is the disparity in the current-voltage relationships of the two samples under the pulsed H.V. and under the DC H.V. (Figure 6(a) and (b)).

On the one hand, all the Fowler-Nordheim (FN) plots (Figure 6 insets) show good linearity, indicating that the FN tunneling theory still worked under the pulsed H.V. condition. Therefore, the response of an emitter to a H.V. pulse can be approximately divided into four consecutive processes: (1) the charging at the beginning of the pulse; (2) the occurrence and the subsequent dramatic decay of field emission in the first half of the pulse; (3) the stable field emission with slight decay in the second half of the pulse; and (4) the discharging at the end of the pulse.

On the other hand, the field emission currents under pulsed H.V. were clearly larger than those under the DC H.V. Table 2 shows this disparity more quantitatively.

Under the pulsed H.V., when the values of $\frac{V_0}{d}$ were

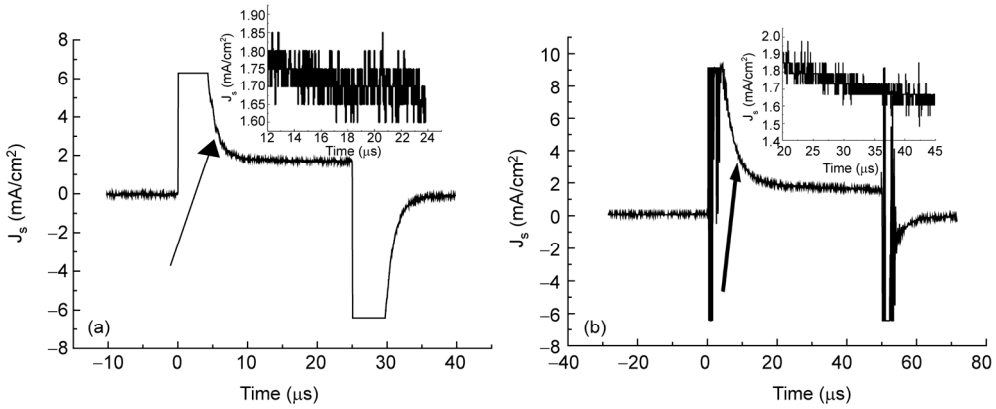

Figure 4 Dependence of the measured current densities on time in individual pulses (insets show the waveforms in the second halves of the pulses). The repetition rate was 200 Hz. (a) MWCNTs; (b) TiO_2 nanotubes.

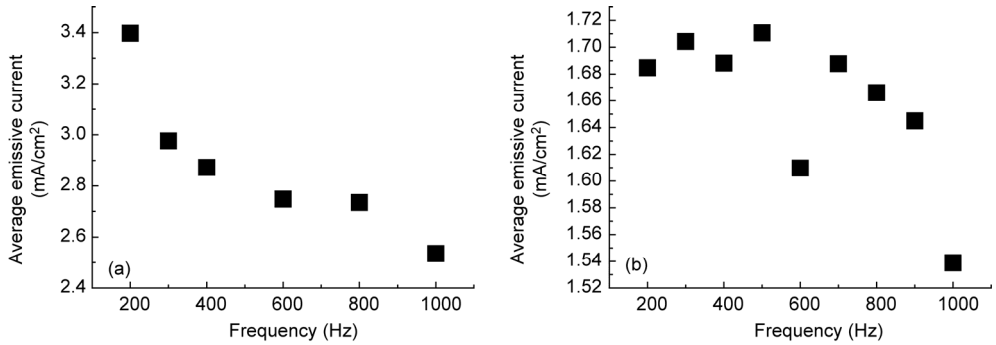

Figure 5 Dependence of the average emissive current on the repetition frequency of the pulses (V_0/d was equal to E_{th} under DC voltages). (a) MWCNTs; (b) TiO_2 nanotubes.

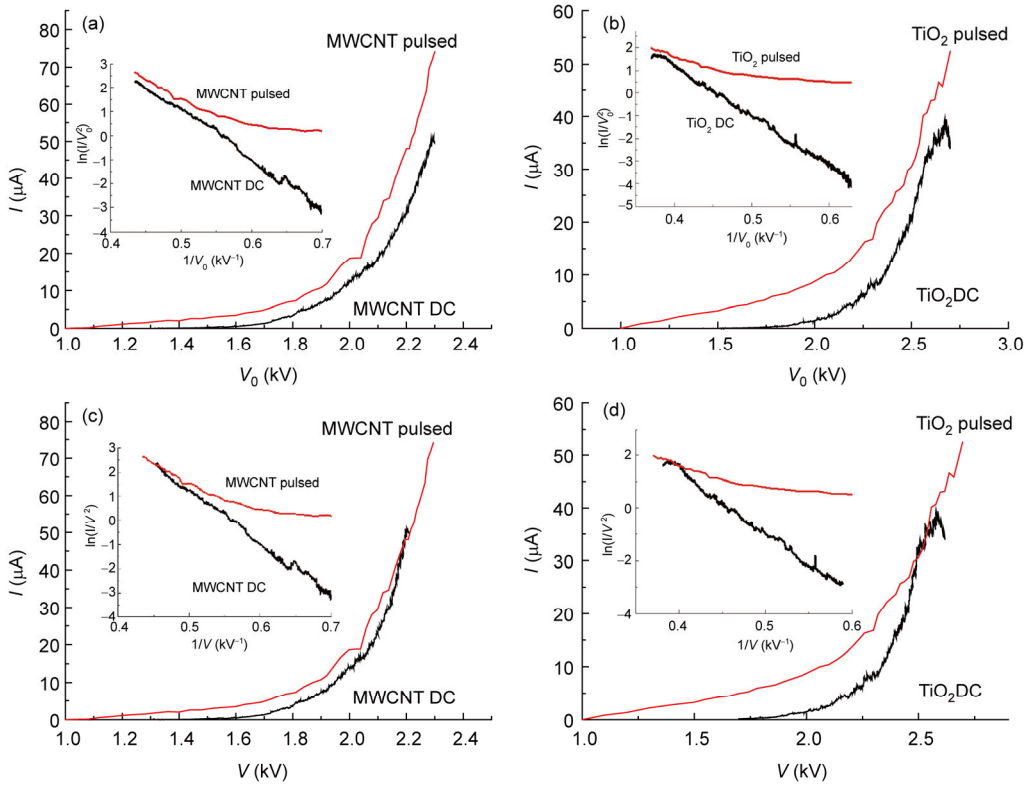

Figure 6 (Color online) Current-voltage curves under the pulsed and DC H.V. The insets are the Fowler-Nordheim plots. V_0, output voltage of the voltage source; V, actual voltage drop across the cathode-anode gap; I, emissive current under DC H.V. or the "average emissive current" under pulsed H.V. (a) I-V_0 curves of the MWCNTs; (b) I-V_0 curves of the TiO_2 nanotips; (c) I-V curves of the MWCNTs; and (d) I-V curves of the TiO_2 nanotubes.

Table 2 Comparison between the field emission under pulsed H.V. and DC H.V.[a)]

Sample	Turn-on and threshold fields (V/μm)			J_P (mA/cm^2) under E_{on}(D)	J_P (mA/cm^2) under E_{th}(D)
	E_{on}(D)	E_{th}(D)	E_{th}(P)		
MWCNTs	6.51	10.2	9.9	0.87	1.85
TiO_2 nanotubes	8.97	13.2	12.7	0.75	1.27

a) E_{on}(D) and E_{th}(D), turn-on fields and threshold fields under DC voltages, respectively; E_{th}(P), threshold fields under pulsed voltages; J_P, current density under pulsed voltages when the values of $\frac{V_0}{d}$ were equal to E_{on}(D) or E_{th}(D).

equal to the DC turn-on electric fields, the emissive current densities from the MWCNTs and TiO_2 nanotubes were 87 and 75 times their counterparts under the DC H.V. (10 μA/cm^2), respectively (Table 2). Whereas when the values of V_0/d were equal to the DC threshold electric fields, the emissive current densities from the MWCNTs and TiO_2 nanotubes were 85% and 27% higher than their counterparts under the DC H.V. (1 mA/cm^2), respectively.

The results shown in Figures 4–6 can all be attributed to the increase of the R value caused by the temperature rise during the field emission. The field emission current gave rise to Joule heat both in the cathode and at the cathode-substrate interface. As the time elapsed in a pulse, a larger portion of voltage had to fall in the cathode and across the cathode-substrate interface with the rising temperature. When the repetition frequency was higher, the heat diffusion became less timely. This resulted in a decrease of emissive current. The DC voltage could be treated as the extreme condition of increasing the repetition frequency, and thus the disparity between the DC emission and pulsed emission was considerable.

The R values under the DC voltages can be estimated in a semiquantitative manner. For this purpose, the "actual" voltage across the cathode-anode gap must be introduced:

$$V = V_0 - IR, \tag{6}$$

where V_0 denotes either the magnitude of the square-wave pulses from the pulsed voltage source or the output voltage from the DC voltage source; I denotes the emissive current under the DC voltages and the "average emissive current" under the pulsed voltages, as defined previously.

As shown in Figure 6(a) and (b), for both samples, if the abscissa of the current-voltage curves is set to V_0, the curves obtained under the DC voltages are to the right of those obtained under the pulsed voltages. Because of the sustained heating caused by the passage of current under the DC voltages, the values of R in the circuits (Figure 2) are clearly larger under the DC voltages than under the pulsed voltages, and thus smaller voltages are available across the cathode-anode gap. In Figure 6(c) and (d), the abscissa is changed from the voltage source output (V_0) to the actual voltage across the cathode-anode gap (V). For the case of the pulsed voltages, we used the R values given in Table 1: 70 kΩ for the MWCNTs, and 75 kΩ for the TiO_2 nanotubes. For the case of the DC voltages, we performed iterative fitting, and the R values were set to 1.8 MΩ for the MWCNTs and 2.4 MΩ for the TiO_2 nanotubes. After this modification of the abscissa, as shown in Figure 6(c) and (d), the pulsed voltage MWCNT curve and the DC voltage MWCNT curve almost coincide, and the two TiO_2 curves also approach each other. As shown in Figure 4, under the pulsed voltages, the fluctuation and attenuation of the emissive current from the TiO_2 nanotubes were considerable, i.e., the currents clearly deviated from the "average emissive current." Furthermore, "R" was not a constant with increasing V_0. Probably for these two reasons, the two TiO_2 I-V curves shown in Figure 6(d) do not coincide well with each other when the voltages were not high.

The above results show that the requirements for the parameters of the cathode-anode system working under pulsed voltages are in conflict with those under DC voltages in some aspects. Under DC voltages, the cathode-anode separation should be as small as possible so that a moderate voltage can generate a strong electric field. However, because the capacitance is inversely proportional to this separation, a too small separation means a large time constant and thus a considerable delay in the current response. Moreover, under DC voltages, the smaller the R value, the less the voltage drop on the emitter. However, under pulsed voltages, if the R is too small, the charging current might be sufficiently large to constitute a threat to some of the components in the circuit.

The current-voltage curves obtained under the DC voltages (Figure 6(c) and (d)) are also used to estimate the field enhancement of the two emitters. We use the most simplified form of the FN theory [18]:

$$J = AE^2 \exp\left(-\frac{B\phi^{\frac{3}{2}}}{E}\right), \quad I = JS, \tag{7}$$

where J and I are the local field emission current density and field emission current, respectively; ϕ is the work function; E is the local electric field at the actual emission sites; S is the total area involved in the field emission; and A and B can be approximated by two constants.

Because E cannot be measured directly, it is usually calculated by

$$E = \beta\frac{V}{d} = \beta\frac{(V_0 - IR)}{d}, \tag{8}$$

where d is the cathode-anode separation, and β is the field enhancement factor. As defined above, here V and V_0 denote the actual voltage across the cathode-anode gap and the output voltage of the voltage source, respectively. Thus $\frac{V}{d}$ is the average field between the cathode and the anode.

Therefore, the relationship between the field emission current and the cathode-anode gap voltage is written as

$$I = SA\beta^2\frac{V^2}{d^2}\exp\left(-\frac{Bd\phi^{\frac{3}{2}}}{\beta V}\right). \tag{9}$$

With the ϕ values set to 4.95 and 4.2 eV [19,20], the β values were calculated to be 7×10^3 and 5×10^3 for the MWCNTs and the TiO_2 nanotubes, respectively. The fact that the field enhancement factor of the MWCNTs was larger than that of the TiO_2 nanotubes is within expectations, because the aspect ratio of the MWCNTs should be larger.

4 Conclusion

A field emitter behaves differently under pulsed voltages than under DC voltages. First, the displacement current also contributes to the current measured in the circuit, and the

waveform of the voltage across the cathode-anode gap is greatly distorted by the charging process. Second, higher emissive current can be extracted by a pulsed voltage than by a DC voltage. However, the decay of the emissive current within a pulse is considerable, particularly at the beginning of the pulse.

Consequently, special requirements are imposed on the emitters and cathode-anode systems that operate under pulsed voltages, which might contradict the requirements for the emitters and cathode-anode systems that operate under DC voltages. In this sense, suitable compromises are necessary, which may include (1) a low cathode-anode voltage and a small voltage waveform distortion and (2) a low-voltage drop on the emitter and a small displacement current.

The authors benefited greatly from visiting the laboratories of Prof. Wei Lei (Southeast University) and Dr. Yu Zhang (Sun Yat-sen University). This work was supported by the Ministry of Science and Technology of China (Grant No. 2013CB933604).

1 Xu N S, Huq S E. Novel cold cathode materials and applications. Mater Sci Eng R Rep, 2005, 48: 47–189
2 Spindt C A. A thin-film field-emission cathode. J Appl Phys, 1968, 39: 3504–3505
3 Baughman R H, Zakhidov A A, de Heer W A. Carbon nanotubes—The route toward applications. Science, 2002, 297: 787–792
4 Lee C J, Lee T J, Lyu S C, et al. Field emission from well-aligned zinc oxide nanowires grown at low temperature. Appl Phys Lett, 2002, 81: 3648–3650
5 Zhu Y W, Zhang H Z, Sun X C, et al. Efficient field emission from ZnO nanoneedle arrays. Appl Phys Lett, 2003, 83: 144–146
6 Chen J, Deng S Z, Xu N S, et al. Temperature dependence of field emission from cupric oxide nanobelt films. Appl Phys Lett, 2003, 83: 746–748
7 Hsieh C T, Chen J M, Lin H H, et al. Field emission from various CuO nanostructures. Appl Phys Lett, 2003, 83: 3383–3385
8 Wang L, Wei G, Gao F, et al. High-temperature stable field emission of B-doped SiC nanoneedle arrays. Nanoscale, 2015, 7: 7585–7592
9 Wang L, Li C, Yang Y, et al. Large-scale growth of well-aligned SiC tower-like nanowire arrays and their field emission properties. ACS Appl Mater Interface, 2015, 7: 526–533
10 Wei G, Liu H, Shi C, et al. Temperature-dependent field emission properties of 3 C-SiC nanoneedles. J Phys Chem C, 2011, 115: 13063–13068
11 Choi W B, Chung D S, Kang J H, et al. Fully sealed, high-brightness carbon-nanotube field-emission display. Appl Phys Lett, 1999, 75: 3129
12 Yue G Z, Qiu Q, Gao B, et al. Generation of continuous and pulsed diagnostic imaging X-ray radiation using a carbon-nanotube-based field-emission cathode. Appl Phys Lett, 2002, 81: 355–357
13 Teo K B K, Minoux E, Hudanski L, et al. Microwave devices: Carbon nanotubes as cold cathodes. Nature, 2005, 437: 968–968
14 Matheson R M, Nergaard L S. The decay and recovery of the pulsed emission of oxide-coated cathodes. J Appl Phys, 1952, 23: 869–875
15 Li S, Zhang G, Guo D, et al. Anodization fabrication of highly ordered TiO_2 nanotubes. J Phys Chem C, 2009, 113: 12759–12765
16 Liang J, Zhang G. TiO_2 nanotip arrays: Anodic fabrication and field-emission properties. ACS Appl Mater Interface, 2012, 4: 6053–6061
17 Bonard J-M, Maier F, Stöckli T, et al. Field emission properties of multiwalled carbon nanotubes. Ultramicroscopy, 1998, 73: 7–15
18 Gomer R. Field Emission and Field Ionization. Cambridge: Harvard University Press, 1961
19 Shiraishi M, Ata M. Work function of carbon nanotubes. Carbon, 2001, 39: 1913–1917
20 Imanishi A, Tsuji E, Nakato Y. Dependence of the work function of TiO_2 (rutile) on crystal faces, studied by a scanning auger microprobe. J Phys Chem C, 2007, 111: 2128–2132